The power law statistics of the spiking timing in a neuronal network

Chenggui Yao [a,b], JianQiang Sun [c], Jun Jin [d], Jianwei Shuai [d,b], Xiang Li [d,*], Yuangen Yao [e,*], Xufan Xu [f]

[a] College of Data science, Jiaxing University, Jiaxing, 314000, China
[b] Wenzhou Key Laboratory of Biophysics, Wenzhou Institute, University of Chinese Academy of Sciences, Wenzhou, 325000, China
[c] School of Automation and Electrical Engineering, Linyi University, Linyi, 276000, China
[d] Department of Physics, and State Key Laboratory of Cellular Stress Biology, Innovation Center for Cell Signaling Network, Xiamen University, Xiamen, 361102, China
[e] School of science, Huazhong Agricultural University, Wuhan, 430000, China
[f] College of Material and Textile Engineering, Jiaxing University, Jiaxing, 314000, China

ARTICLE INFO

ABSTRACT

Information encoding and decoding by neurons is a fundamental process in neuroscience. Herein, we present a statistical investigation of the first spike timing arising from the neuronal population in a small-world network with the Hodgkin–Huxley model after a neuron has received current stimulation, including a transient or a continuous stimulus. Regardless of how the interaction between neurons in the network was implemented, via electrical coupling or chemical synapses, we found the same power-law statistics for the first spike timing, independent of the topological structure of the neuronal network. We further suggest that such power-law statistics can be a generalized feature for the first spike timing in the small-world and scale-free neuronal networks. Our findings provide new insight into the coding mechanism for the first spike timing and improve the understanding of the power-law behavior in nature.

1. Introduction

One of the most important research problems in neuroscience is understanding the coding mechanism. Stimulus information is encoded in action potentials (AP) or spikes when the total dendritic input reaches a threshold, and neurons exchange information via stereotyped pulses. It is accepted that information may be encoded following two different encoding mechanisms: the mean firing rate (firing rate coding) and spike timing (temporal coding). The firing rate coding is statistically computed based on the number of spikes in a fixed time window, and the information about the stimulus is then encoded in the firing rate of the neuron [1–3]. In the firing rate coding, the spike count is positively correlated to the stimulus intensity, while this is not the case for the temporal coding since the precise spike timing and coordination in time are considered [4]. Although there is still a controversy about the firing rate or temporal code, the spike timing has received increased research attention over the past decades due to growing evidence of the relation between synchronization in neural networks and higher brain functions, such as memory, attention, and cognition [5,6]. Signal encoding, transmission, and decoding play a crucial role in neuron-related computation, learning, and cognitive processing, and their various aspects have been systematically investigated [7–12].

Under strong temporal constraints, the first spikes per neuron could also encode and process information [4]. The first-spike coding, using the first-spike latency as an information carrier, was first proposed by Hopfield [4], followed by many experiments performed in vertebrates [13–15] and invertebrates [16,17]. The first-spike latency is a robust and reliable measure of the neural response delay since it carries more information than other spikes [18]. The important findings supporting the neurophysiological meaning of first spike encoding are the experimental observations that neurons in the brain exhibit temporal precision for their spiking patterns. For example, neurons in the auditory system can detect differences in the timing of sound stimuli with millisecond precision [19]. Similarly, neurons in the visual system are able to encode information about the timing of visual stimuli with submillisecond precision [20]. In addition, the first-spike latency can also successfully identify the stimulus form in auditory [21,22], visual [23,24] and somatosensory [25,26] systems. The responding dynamics of the first-spike latency of neurons was investigated theoretically and computationally [27–29]. For example, an analytical approach was provided to determine the spike timing from a given initial state in two different neuronal models [30]. Pankratova et al. studied the influence of noise on the spike timing of a single

---

* Corresponding authors.
E-mail addresses: xianglibp@xmu.edu.cn (X. Li), yyg@mail.hzau.edu.cn (Y. Yao).

neuron subjected to a suprathreshold periodic forcing and found that the mean latency nonmonotonically depends on the noise strength. This phenomenon, named noise delayed decay (NDD) [31,32], was then investigated widely under different conditions to explore the biophysical mechanisms of the first-spike latency [33–39]. Furthermore, researchers have observed a fascinating phenomenon known as "chaos delayed decay" (CDD), whereby the first spike latency of a deterministically forced Hodgkin–Huxley neuron exhibits a significant delay that depends on the intensity of chaotic current. Interestingly, the firing rate of the neuron demonstrates a non-monotonic relationship with the intensity of the chaotic current [40].

In this work, we addressed how the information is estimated by analyzing the distribution of first spike timing in the neural population. Using Hodgkin–Huxley neurons with small-world coupling, we investigated the probability distribution of first spike timing, which originated from the neuronal network. Our results show that the probability distribution follows a power law and exhibits universal features for the small world network and scale free network with several parameter settings. Remarkably, the distribution of first spike timing is independent of the type of synapse, the type of stimulus, and the topological structure of the network. This paper is organized as follows: Section 2 presents the Hodgkin–Huxley neuronal network model and the analytical method. Section 3 shows the main results under different conditions. Finally, our conclusions are summarized in Section 4.

2. Models and methods

To simulate the time evolution of the action potential of a neuron in the neuronal network, we employed the coupled Hodgkin–Huxley neuron model [41–43]:

$$C_m \frac{dV_i}{dt} = -(G_i^K(n_i)(V_i - V_K) + G_i^{Na}(m_i, h_i)(V_i - V_{Na}) + G_i^L(V_i - V_l)) \quad (1)$$
$$+ \delta_{i,d} I_{stim} + I_{syn}^i,$$

where V_i stands for the membrane potential of the ith neuron in millivolts, $i = 1, 2, \ldots, N$, and $C_m = 0.75$ μF/cm^2 denotes for the membrane capacitance per unit area. $V_{Na} = 60.0$ mV, $V_K = -90.0$ mV, and $V_l = -70.0$ mV are the reversal potentials for sodium, potassium and leak channels, respectively. In our model, the leak conductance G_i is assumed to be constant ($G_i = g_L = 0.033$ mS/cm^2), while the sodium and potassium conductances depend on the gating variables according to the following equations:

$$G_i^{Na}(m_i, h_i) = g_{Na}^{max} m_i^3 h_i, \qquad G_i^K(n_i) = g_K^{max} n_i, \quad (2)$$

where $g_{Na}^{max} = 150.0$ mS/cm^2 and $g_K^{max} = 40.0$ mS/cm^2 represent the maximal sodium and potassium conductances, respectively. The gating variable for activation and inactivation which regulates the sodium current are denoted by m_i and h_i, respectively, and n_i is the activation gating variable for the potassium current. These gating variables can be written unanimously as:

$$\frac{dm_i}{dt} = \frac{1}{\tau_{m_i}}(-m_i + m_i^\infty), \quad \tau_{m_i} = \frac{1}{\alpha_{m_i} + \beta_{m_i}}, \quad m_i^\infty = \frac{\alpha_{m_i}}{\alpha_{m_i} + \beta_{m_i}}, \quad (3)$$

$$\frac{dn_i}{dt} = \frac{1}{\tau_{n_i}}(-n_i + n_i^\infty), \quad \tau_{n_i} = \frac{1}{\alpha_{n_i} + \beta_{n_i}}, \quad n_i^\infty = \frac{\alpha_{n_i}}{\alpha_{n_i} + \beta_{n_i}},$$

$$\frac{dh_i}{dt} = \frac{1}{\tau_{h_i}}(-h_i + h_i^\infty), \quad \tau_{h_i} = \frac{1}{\alpha_{h_i} + \beta_{h_i}}, \quad h_i^\infty = \frac{1}{1 + e^{(V_i+60)/6.2}},$$

$$\alpha_{m_i} = \frac{0.142(V_i + 30)}{1 - e^{-(V_i+30)/8}}, \qquad \beta_{m_i} = -\frac{0.097(V_i + 30)}{1 - e^{-(V_i+30)/8}},$$

$$\alpha_{n_i} = \frac{0.0078(V_i - 30)}{1 - e^{-(V_i-30)/9}}, \qquad \beta_{n_i} = -\frac{0.00156(V_i - 30)}{1 - e^{-(V_i-30)/9}},$$

$$\alpha_{h_i} = \frac{0.022(V_i + 45)}{1 - e^{-(V_i+45)/6}}, \qquad \beta_{h_i} = -\frac{0.0071(V_i + 70)}{1 - e^{-(V_i+70)/6}}.$$

I_{syn}^i in Eq. (1) is the total synaptic current received by neuron i. The coupling via electrical gap junctions and chemical synapses is considered in our work. The interaction between neurons, whether it is through electrical coupling or chemical synapses, plays a critical role in the coding of neural information. The precise timing and strength of synaptic connections between neurons can encode specific information, such as sensory input or memory formation. Studies have shown that the precise timing of action potentials and the strength of synaptic connections can lead to the formation of spatiotemporal patterns of activity, which are thought to be important for information processing and computation in the brain [44,45]. The synaptic current via electrical gap junctions is directly proportional to the difference in action potential between neuron i and that of the neighbored neuron, averaged over neighbors:

$$I_{syn}^i = \epsilon \sum \frac{g_{i,j}}{k_i}(V_j - V_i), \quad (4)$$

where ϵ is the conductance of the gap junction. For the chemical synapses, the synaptic current is described as follows:

$$I_{syn}^i = g_c \sum \frac{g_{i,j}}{k_i} \alpha_{syn}(t - t_0^j)(V_{rev} - V_i), \quad (5)$$

where the alpha function $\alpha_{syn}(t) = \frac{t}{\tau_{syn}} e^{-\frac{t}{\tau_{syn}}}$ is the synaptic conductance function, $\tau_{syn} = 2$ ms. g_c is the maximal conductance of the synaptic channel, and t_0^j is the time when presynaptic neuron j spikes. The parameter V_{rev} is synaptic reversal potential, and it determines the type of synapse. Herein, we only consider the excitatory synapses by setting $V_{rev} = 0.0$. The factors $g_{i,j}$ are given by $g_{i,j} = 1(g_{j,i} = 1)$ when the neuron j is the neighbor of node i, and otherwise $g_{i,j} = 0$. The number of the neighbor i can be computed by $k_i = \sum_{j=1}^{N} g_{i,j}$. The stimulus current $I_{stim} = 40$ μA/cm^2 with a 2 ms duration time is sent to one randomly chosen neuron. To avoid the influence of initial conditions on the spike timing, the stimulus is added after the systems have evolved 200 ms. The stimulus current is sent to a single neuron by setting $\delta_{i,d}$, where d is an index of the simulated neuron. $\delta_{i,d} = 1$ when $i = d$, otherwise, $\delta_{i,d} = 0$.

We focus on the topology of the neurons with the small-world networks, since the small-world properties are ubiquitous in the established and reconstructed structural and functional brain networks [46–51]. It was proposed by Watts and Strogatz, characterized by a high clustering coefficient and short path length [52]. Small-world structure is an excellent model for brain network due to the segregated and distributed information processing [53,54]. We also used a standard algorithm to build a small-world network, i.e., we started with a neighboring-connected ring with periodic boundary conditions. With the probability p_s, we disconnected an edge and reconnected it to a vertex chosen uniformly from the entire ring; the process was then repeated for each node [52].

To evaluate the response latency dynamics of neurons, we defined T_i as the spike timing when an AP crosses a threshold, here equal to 0 mV; then, the latency time t_i of each neuron is defined as the difference between the T_i of each neuron and that of the stimulated one. We analyzed the probability distribution of t_i. To evaluate the probability distribution, a histogram was used first. Then, we used a quantile–quantile plot which is a powerful technique for checking the validity of a distributional assumption for a data set. The basic idea is to compare the quantile of each data item with the theoretical quantile based on the hypothetical distribution. If the data matches the assumed distribution, the points should approximately approach a straight line in the quantile–quantile plot. Finally, we conducted a Kolmogorov–Smirnov test on the distribution. The return logical value $h = 1$ or 0 stands for rejecting or accepting the null hypothesis, respectively. The return p-value of the test is the probability of observing the test statistics under the null hypothesis. The validity of the null hypothesis is in doubt due to small p-values. The significance level α is 0.05 [55]. The model was integrated numerically using the fourth-order Runge–Kutta algorithm with a fixed temporal resolution of 0.01 ms. The initial conditions v_i^0 are chosen randomly from $[-100, 20]$, m_i^0, n_i^0, and h_i^0 are chosen randomly from $[0, 1]$.
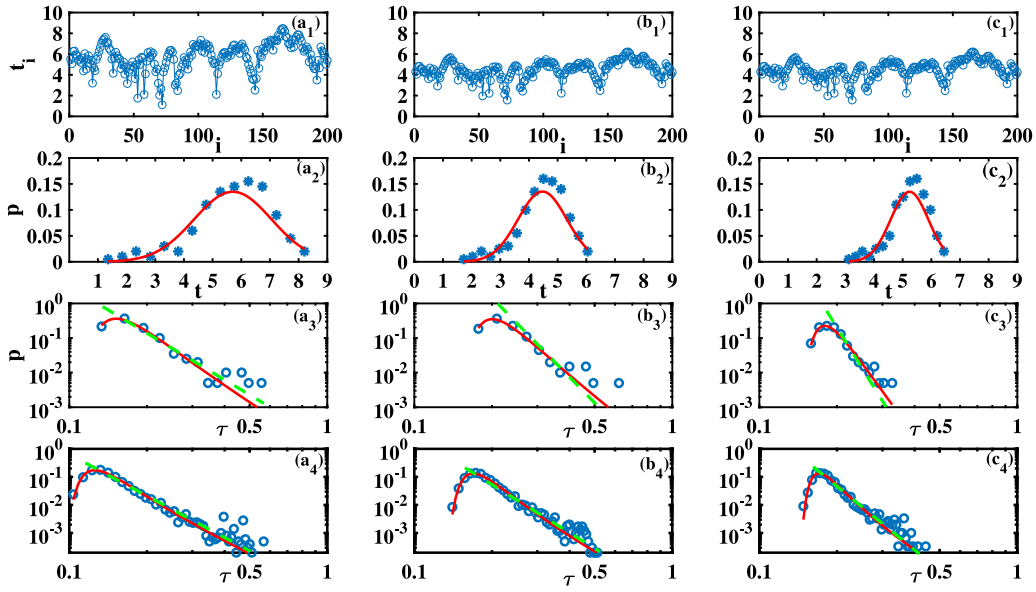
Fig. 1. (Color online) (a$_1$)–(c$_1$) The latency t_i in the small-world neuronal network with $N = 200, p_s = 0.3$ for the coupling strength $\epsilon = 1.0, 2.0,$ and 3.0, respectively. (a$_2$)–(c$_2$) The probability p for the first spiking latency t for different coupling strength. (a$_3$)–(c$_3$) The probability p scales as a power law with τ ($\tau = \frac{1}{t}$) for different coupling strengths; (a$_4$)–(c$_4$) The probability p vs τ for 100 small-world network samples for different coupling strengths. The solid lines show the maximum likelihood fit while the dash lines are for the least square method. For the columns from left, middle to right, $\epsilon = 1.0, 2.0,$ and 3.0, respectively.

3. Results for networks with a transient stimulus

Networks with electrical synapses

First, we consider that the neuronal network is stimulated by a transient stimulus current with a 2 ms duration time, and one randomly chosen neuron is activated. Figs. 1(a$_1$)-(c$_1$) show the response time t_i in the small-world neuronal network for different coupling strengths. The latency time t_i is random for different coupling strengths. Also, the smaller the coupling strength, the stronger the fluctuation. In particular, Figs. 1(a$_2$)-(c$_2$) illustrate the probability distributions p for t_i with $\epsilon = 1.0, 2.0$ and 3.0, respectively, where the data t_i is generalized as t. These distributions are single-peaked and rightward. However, a rightward distribution model is rare. Then, we set $\tau = \frac{1}{t}$, and probability p for τ are shown in Figs. 1(a$_3$)-(c$_3$), now becoming leftward. Strikingly, the probability distributions show an excellent fit to a power law, validated by the test of the maximum likelihood estimator (the solid line in Figs. 1(a$_3$)-(c$_3$)). To test the power law of probability distributions, 100 small-world networks with $N = 200$ samples were generated, and a stimulated neuron was randomly chosen. Then, 20,000 records for t_i were generated. The probability distributions p for τ are presented in Figs. 1(a$_4$)-(c$_4$), respectively. The leftward probability distribution can be clearly observed from the three subfigures. The numerical experiments show a clear power law relation between $\ln p$ and $\ln \tau$, i.e.,

$$\ln p \propto \alpha \ln \tau. \tag{6}$$

So far, all these findings indicate the power law of probability distributions, which was considered ubiquitous in physics and life sciences for a long time. However, the nature of the probability distribution model, in Fig. 1, remains unanswered, and it is not known whether all data follow the same probability model. To answer these equations, we firstly tested the distribution of these data by plotting quantile–quantile figures. Figs. 2(a)–(f) illustrate quantile–quantile plots for matching the actual value with the Exponential, Normal, Lognormal, Weibull, Gamma, and Generalized extreme value (GEV) distributions, respectively. Comparing these quantile–quantile plots clearly shows that the data approach to the Exponential distribution and GEV distribution (the red line indicates a perfect correlation), while many data deviate (the
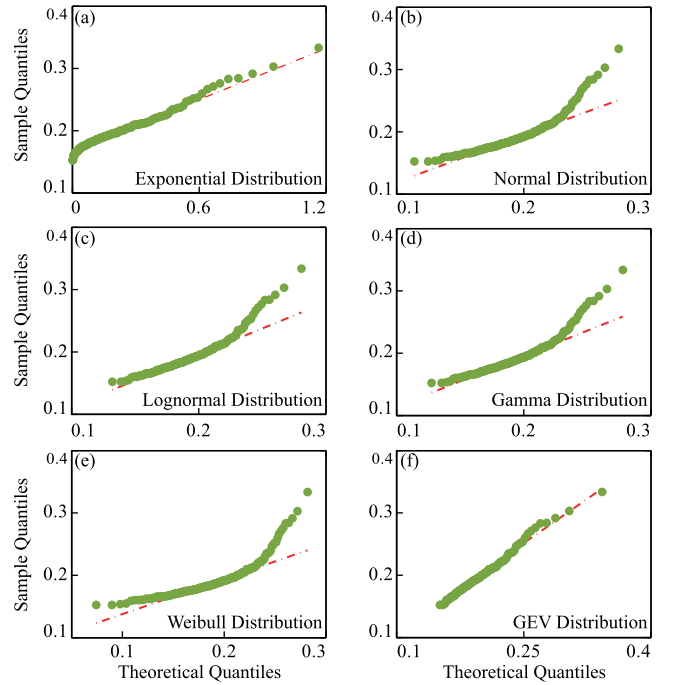
Fig. 2. (Color online) (a)–(f) Quantile–quantile plots that match the actual values with the following distributions respectively: Exponential (The probability density function $p(x) = \lambda e^{-\lambda x}$), Normal (The probability density function $p(x) = \frac{1}{\sqrt{2\pi}\sigma} e^{-\frac{(x-\mu)^2}{2\sigma^2}}$), Lognormal (The probability density function $p(x) = \frac{1}{\sqrt{2\pi}\sigma x} e^{-\frac{(\ln x - \mu)^2}{2\sigma^2}}$), Gamma (The probability density function $p(x) = \frac{\lambda^\alpha}{\Gamma(\alpha)} x^{\alpha-1} e^{-\lambda x}$ λ is the scale parameter, k is the shape parameter $\Gamma(x)$ is the Γ function), Weibull (The probability density function $p(x) = \frac{k}{\lambda}(\frac{x}{\lambda})^{k-1} e^{-(\frac{x}{\lambda})^k}$ λ is the scale parameter, k is the shape parameter), and Generalized extreme value distribution (GEV) (The probability density function $p(x) = e^{f(x)} f'(x), f(x) = -(1 + k\frac{x-\mu}{\sigma})^{-\frac{1}{k}}$, μ is the location parameter, σ is scale parameter, and k is the shape parameter).
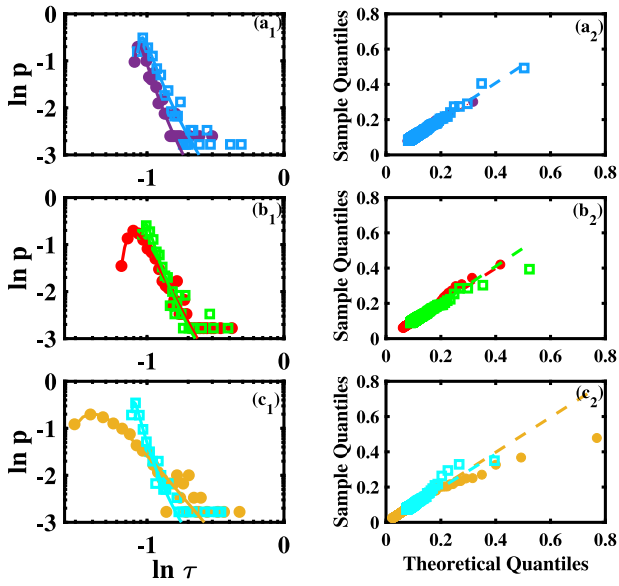
Fig. 3. The probability p versus τ in different settings. (a_1) different size N ($N = 400$ (the purple points) and 600 (blue squares)) with $p_s = 0.3, \langle k \rangle = 4$. ($b_1$) different connect probability p_s ($p_s = 0.1$ (red points), 0.5 (green squares)) with $N = 600, \langle k \rangle = 4$. ($c_1$) different average degree $\langle k \rangle$ ($\langle k \rangle = 2$ (the dark-yellow points) and 6 (cyan squares)) with $p_s = 0.3, N = 600$. (a_2)-(c_2) The dashed lines show the power law function by the least square method. The quantile–quantile plots for the hypothesis of GEV distribution correspond to (a_1)-(c_1), respectively. (For interpretation of the references to color in this figure legend, the reader is referred to the web version of this article.)

red line for other distribution assumptions). We used the Kolmogorov–Smirnov test to check whether the data obey the GEV distribution or Exponential distribution. A logical value $h = 0$ and a p value $p > 0.98$ with a significance level $\alpha = 0.05$ were obtained for the GEV distribution hypothesis, while $h = 0$ and $p = 0.0001$ with the same significance were obtained for the Exponential distribution. Therefore, we reasonably reject the Exponential distribution hypothesis and accept the GEV distribution hypothesis.

To check the universal scaling of the latency in small-world neuronal networks, many examples were tested, including the small-world networks with different sizes N, different connect probabilities p_s, and different average degrees $\langle k \rangle$. These results are shown in Figs. 3 (a_1)-(c_1). These power law behaviors are universal for the small-world neuronal network, as several system parameters have been systematically tested and all qualitative results were unchanged. These results indicate a universal form of the first spiking timing latency which emerging from the small-world neuronal network with electrical synapses.

To further assess our assumption about the GEV distribution, Figs. 3 (a_2)-(c_2) present the best matching between the GEV distribution and the actual values for the small-world networks of different sizes, connect probabilities, and average degrees. The subfigures show that the data fully approach the respective straight line for the different network structures, where only some of them deviate, indicating that the random latency t_i in the small-world neuronal network obeys the same probability distribution (the GEV distribution). Using the Kolmogorov–Smirnov test to check the data in Fig. 3, we get $h = 0$ and a large return p-value [See Table 1]. Thus, we tested the hypothesis that all data follow the GEV distribution and validated the hypothesis. Hence, we conclude boldly that the distribution for the latency, as the first spiking originating from the small-world network with an electrical synapse type, exhibits a power-law property and obeys the GEV distribution. The probability density function of the GEV distribution is given as follows:

$$p(\tau) = e^{f(\tau)} f'(\tau), \quad f(\tau) = -(1 + k \frac{\tau - \mu}{\sigma})^{-\frac{1}{k}}, \tag{7}$$
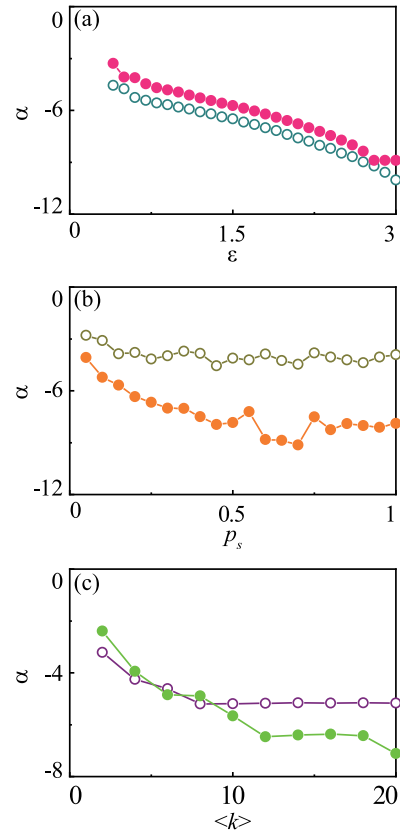
Fig. 4. The power exponent α which is fitted by the least square method against the coupling strength ϵ, the connection probability p_s, and the average degree $\langle k \rangle$ of a small-world network, respectively. In (a) $N = 200, \langle k \rangle = 4$, the dark cyan and pink line corresponds to $p_s = 0.3$ and 0.7, respectively, In (b) $N = 200, \langle k \rangle = 4$, the dark yellow and orange line corresponds to $\epsilon = 0.5$ and 2.5, respectively, In (c) $N = 200, p_s = 0.3$, the purple and green line corresponds to $\epsilon = 0.5$ and 2.5, respectively. (For interpretation of the references to color in this figure legend, the reader is referred to the web version of this article.)

Table 1

The return p-value for KS test.

Synapse type	$N = 400, 600$	$p_s = 0.1, 0.5$	$< k > = 2, 6$
Electrical junction	$p = 0.98, 0.92$	$p = 0.87, 0.89$	$p = 0.90, 0.73$
Chemical synapse	$p = 0.79, 0.91$	$p = 0.83, 0.95$	$p = 0.72, 0.99$

where μ is the location parameter, σ is the scale parameter, and k is the shape parameter. Consequently, we can get the distribution of the first spiking timing based on the $\tau = \frac{1}{t}$. The probability density function for the spiking timing t is shown as

$$p(t) = e^{f(t)} f'(t) \frac{1}{t^2}, \quad f(t) = -(1 + k \frac{\frac{1}{t} - \mu}{\sigma})^{-\frac{1}{k}}, \tag{8}$$

Finally, we checked the power exponent α computed by the least square fitting under different conditions. Figs. 4 (a)–(c) show the power exponent α against the coupling strength ϵ, the connection probability p_s, and the average degree $\langle k \rangle$ of the small-world network, respectively. The α decreases with ϵ, indicating that the coupling strength can enlarge the probability of a small latency [Fig. 4(a)]; when the average degree $\langle k \rangle$ and the connection probability p_s increase, the value of α decreases first and then oscillates with a small amplitude, implying that the large average degree and connection probability may not influence the latency distribution.

Networks with chemical synapses

Our results show that the latency distribution, as the spiking of electrical synapses, exhibits a power-law property and obeys the GEV
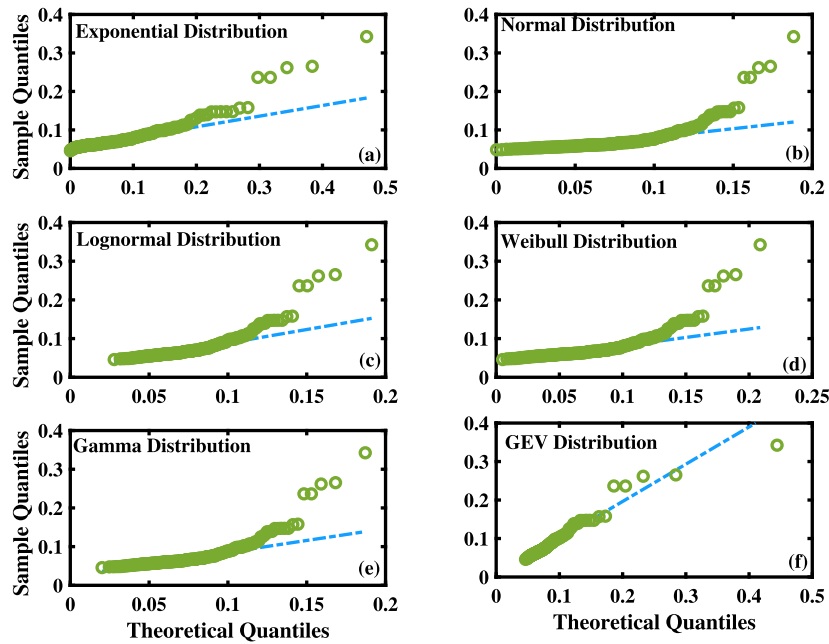
Fig. 5. (Color online) (a)–(f) Quantile–quantile plots that match the actual values with the following distributions, respectively: Exponential, Normal, Lognormal, Weibull, Gamma and Generalized extreme value distribution (GEV). The data for the first spiking were obtained by sampling from a small-world network with chemical synapses under the following conditions: $N = 200, p_s = 0.3, \langle k \rangle = 4$, and $g_c = 1.5$.

distribution. A further question arises, whether this feature exists for the small-world neuronal network with chemical synapses. To determine the optimal distribution for matching the actual values, we generated quantile–quantile plots that compared the data to six candidate distributions: Exponential, Normal, Lognormal, Weibull, Gamma, and Generalized Extreme Value (GEV), as shown in Fig. 5. Upon comparing these subfigures, it became clear that the GEV distribution produced the best match with the data (indicated by a perfect correlation represented by the blue line). Conversely, deviations were observed for other distribution assumptions (indicated by the blue line for those distributions). Further numerical results confirm this, and the power law distribution for τ in the small-world neuronal network with chemical synapses (τ is the inverse of first spiking timing t) is shown in Figs. 6(a$_1$)-(c$_1$) for different chemical synapse weights. Unlike electrical synapses, chemical synapses can lead to delayed interaction, while the coupling of electrical synapses is instantaneous. The chemical synapses may influence the spiking distribution of the neuronal network. The pattern in Fig. 6, however, indicates a surprising result, i.e., the probability scales with the latency following a power law in the same magnitude and obeys the GEV distribution. We also checked three sets of data by using the Kolmogorov–Smirnov test and obtained the logical value $h = 0$ and the return p-value $p = 0.98, 0.77$, and 0.71 with the significance level $\alpha = 0.05$, with all datum following the GEV distribution.

To verify the universality of power laws for the spike latency in a small-world network with chemical synapses, Figs. 7 (a$_1$)-(c$_1$) show the probability p as a function of τ for different network sizes, connection probabilities, and average degrees of the small-world network, respectively. The probability also scales by a power law with τ for the different parameter settings, indicating a universal form of the probability distribution of the spike latency in the small-world network with chemical synapses. Actually, the quantile–quantile plot for the best matching between the GEV distribution and the actual values in Figs. 7 (a$_2$)-(c$_2$) is more convincing for probing the universality of the power law distributions of the spike latency as the spiking in the small-world network with chemical synapses. Using a Kolmogorov–Smirnov test to check the data in Fig. 7, we get the logical value $h = 0$ and the return p-values are large for all data [See Table 1]. Therefore, we infer that
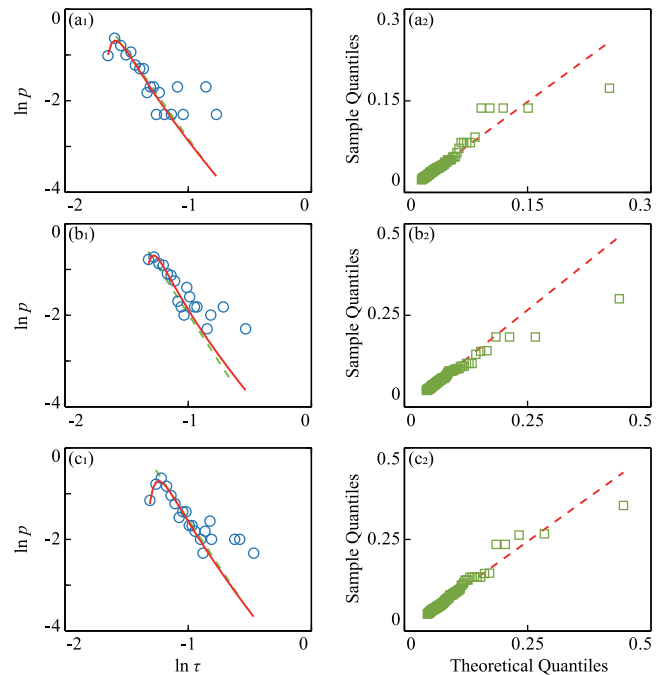
Fig. 6. (Color online) (a$_1$)–(c$_1$) The probability p versus τ for the latency as the first spike in the small-world neuronal network with chemical synapses for the coupling weight $g_c = 0.5, 1.0$, and 1.5, respectively, $N = 200, \langle k \rangle = 4$. The solid line is the maximum likelihood fit. (a$_2$)–(c$_2$) The quantile–quantile plots for the best match between the GEV distribution and the actual values which correspond to (a$_1$)–(c$_1$), respectively.

the first spike latency distribution in a network with chemical synapses exhibits power-law characteristics and obeys the same distribution with electrical gap junctions. Fig. 8 also shows the power exponent α for chemical synapses against the coupling strength g_c, the connection probability p_s, and the average degree $\langle k \rangle$ of the small-world neuronal network. Similar functional relationships can be observed between α
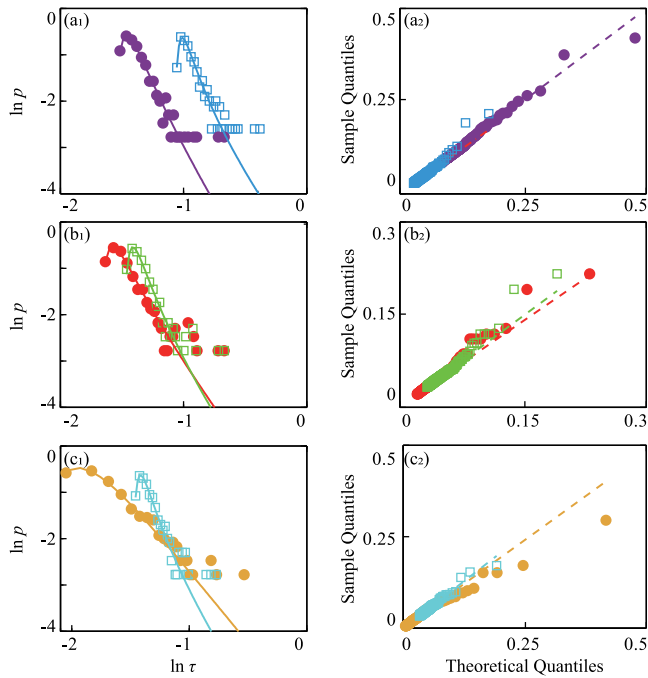
Fig. 7. (a_1)–(c_1) The probability p as a function of τ in small-world neuronal networks with chemical synapses of: (a_1) different size N ($N = 400$ (the purple points) and 600 (blue squares)) with $p_s = 0.3, \langle k \rangle = 4$; ($b_1$) different connect probability p_s ($p = 0.1$ (red points), 0.5 (green squares)) with $N = 600, \langle k \rangle = 4$; and ($c_1$) different average degree $\langle k \rangle$ ($\langle k \rangle = 2$ the dark-yellow points) and 6 (cyan squares)) with $p_s = 0.3, N = 600$. $g_c = 1.0$. (a_2)–(c_2) The quantile–quantile plots for the hypothesis of GEV distribution correspond to (a_1)–(c_1), respectively. (For interpretation of the references to color in this figure legend, the reader is referred to the web version of this article.)

Table 2
The return p-value for the KS test with 5 spikes.

Synapse type	i = 1	i = 2	i = 3	i = 4	i = 5
Electrical junction	$p = 0.90$	$p = 0.57$	$p = 0.8$	$p = 0.59$	$p = 0.92$
Chemical synapse	$p = 0.88$	$p = 0.76$	$p = 0.98$	$p = 0.98$	$p = 0.98$

and ϵ, p_s, and $\langle k \rangle$ as for electrical synapses, indicating that chemical synapses may not influence the distribution type of the spiking of neuronal networks. However, we also find that the value of α for chemical synapses is higher than that of electrical synapses.

4. Results for networks with a continuous stimulus

Actually, it is worth noting that the time-varying stimulus is important for the coding mechanism, and is also an object of interest in several other important fields [56–58]. In particular, we want to study the first-spiking coding mechanism underlying the time-varying stimulus, and to verify whether the universality of power laws for the latency which is induced by the time varying stimulus also holds in this case. With this aim, we consider a stimulus in the form $A\cos(\omega t) + I_0 + \xi(t)$ where $A\cos(\omega t)$ is a weak signal with an amplitude of $A = 0.3$ and a frequency of $\omega = \frac{2\pi}{100}$, $I_0 = 5.0$ is a direct current, and $\xi(t)$ is the Gaussian white noise which satisfies $\langle \xi(t) \rangle = 0.0$, $\langle \xi(t_1)\xi(t_2) \rangle = 2D\delta(t_1 - t_2)$, D is the strength of noise. The stimulus neuron is chosen randomly.

Figs. 9(a) and (b) show the firing patterns in the small-world network with electrical coupling and chemical synapses, respectively. It can be observed that the neurons spike irregularly, and the spike latency per neuron is random. As an example, we first check the latency of the first spiking. The probability p as a function of τ is presented in Figs. 9(c) and (d) for different types of synapses. Clearly, p scales by a power law with τ. The quantile–quantile plot also checks the probability distributions for the best match between the GEV distribution and
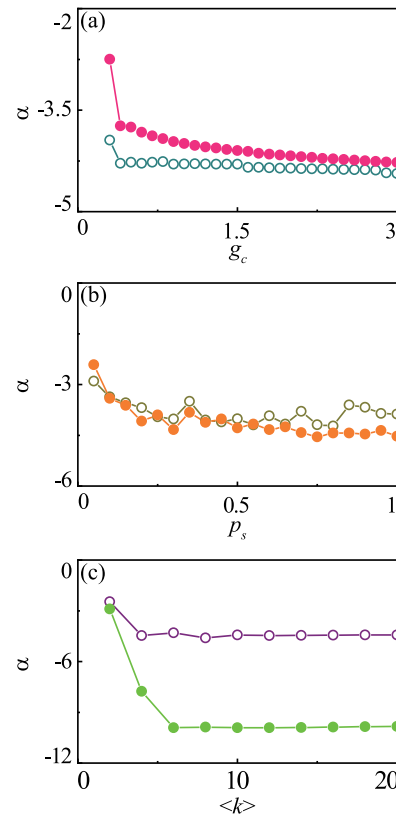
Fig. 8. Comparison of the power exponents α fitted by the least square method versus the coupling strength g_c, the connection probability p_s, and the average degree $\langle k \rangle$ of small-world networks, respectively. In (a) $N = 200, \langle k \rangle = 4$, the dark cyan and pink line corresponds to $p_s = 0.3$ and 0.7, respectively, In (b) $N = 200, \langle k \rangle = 4$, the dark yellow and orange line corresponds to $g_c = 0.5$ and 2.5, respectively, In (c) $N = 200, p_s = 0.3$, the purple and green line corresponds to $g_c = 0.5$ and 2.5, respectively. (For interpretation of the references to color in this figure legend, the reader is referred to the web version of this article.)

the actual values in Figs. 9(e) and (f), respectively. In order to determine the best fit distribution for the data, Figs. 10(a)–(f) also present quantile–quantile plots that compare the actual values to six candidate distributions: Exponential, Normal, Lognormal, Weibull, Gamma, and Generalized Extreme Value (GEV). The blue line in the plots represents perfect correlation between the actual values and the corresponding distribution. Comparing these plots, it is evident that the data most closely approximate the GEV distributions. However, some data points exhibit deviations from the other distribution assumptions. Further, we have applied the Kolmogorov–Smirnov test to check the latencies with arbitrary 5 spikes for both electrical junction and chemical synapse, all the logical values h return to 0 with a large p-value under a significance level of $\alpha = 0.05$ [See Table 2], and all data for spike latency follow the GEV distribution. Therefore, we know that the distribution of the spike latency in neuronal networks may have a power law property and obey the same distribution with the features independent of the type of stimulus. These power law behaviors are universal for the stimulus, as several system parameters of stimulus have been systematically tested and all qualitative results were unchanged.

5. Conclusions and discussions

In this paper, we investigated the probability distribution of the first spike timing latency, originating from the neuronal populations in the small-world network, either with electrical or chemical synapses after a neuron has received a stimulus current, including a transient or a continuous stimulus. We found that the distribution of the random latency
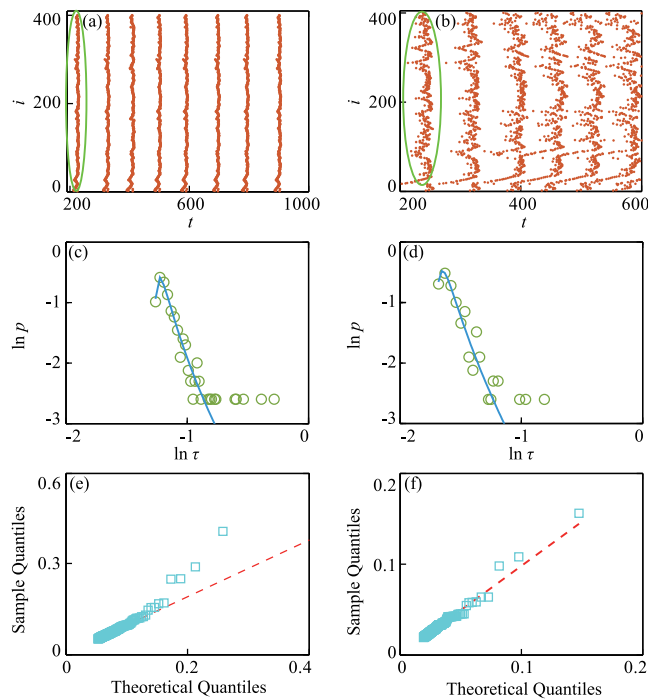
Fig. 9. (Color online) Dot-raster plots of spike times ((a)–(b)), probability ((c)–(d)), and quantile–quantile plots ((e)–(f)) of the latency as the first spiking of small-world neuronal network with time-varying stimulus for $N = 400$, $p_s = 0.3$, $D = 5.0$, ϵ (g_c) = 0.5, respectively. The left and right columns correspond to the electrical coupling and chemical synapses, respectively.

follows a rightward power law and becomes leftward while reversing the random spike timing. To test the data distribution, we used the quantile–quantile plot, which is a powerful statistical tool to compare the actual data with some classical probability model, including the Exponential, Normal, Log-normal, Weibull, Gamma, and GEV distribution. The best matching occurred between the GEV distribution and the actual values, while the data largely deviated in other distributions. Using the Kolmogorov–Smirnov test for all data, we determined that all data obey the GEV distribution, validating the hypothesis. We also assessed the probability of first spike latency of a scale-free network. Unlike the small-world network, the scale-free network exhibited a singularity in the degree distribution (data not shown here). The scale-free network showed a smaller clustering coefficient and larger hubs than the small-world network. Intuitively, the latency distribution in the scale-free neuronal network was different from that of the small-world network. However, a completely opposite result occurred (data not shown here), i.e., the probability scaled as a power law with the latency in the same magnitude in different network parameter settings, also obeying the GEV distribution. Remarkably, this power law behavior appears to be universal. We systematically tested several parameters, including different stimulus currents, stimulus durations, noise strengths, and small-world network structures with varying parameters. Despite these variations, we found that the distribution type remained unchanged, indicating the robustness of the observed power law behavior.

Power law is a statistical concept that describes a functional relationship between two variables where one variable varies as a power of the other. One of the remarkable features of power law is its ability to show the universal characteristics across different systems and disciplines. For example, it has been found that the degree distribution of many real-world networks follows a power law distribution, including the internet, social networks, and biological systems [59,60]. This indicates that there may be potential mechanisms or principles that control the structure and behavior of these systems. Moreover, the power law has been used to study the dynamics of complex systems,

such as the spread of infectious diseases, the occurrence of financial crises, and the evolution of biological systems [61,62]. Researchers can gain insights into the fundamental principles that govern their behavior and make predictions about their future evolution when the universal characteristics of these systems are identified. Power law statistics and its associated universal characteristics have proven to be powerful tools for understanding complex systems in a wide range of disciplines, and further research in this area is likely to yield important insights into the behavior of these systems. Therefore, we believe that our findings are not only of interest to researchers in neuroscience but also valuable in statistical physics.

Although the encoding mechanism used by neurons is still unclear, it is widely accepted that coding is based on action potentials or spikes. This work addresses how to estimate the latency information from the distribution of spike timing when one of the neurons in the neural population is stimulated. Understanding the coding mechanism is an important question in neuroscience, essential to shed light on how the cortex processes and transmits information. Interestingly, the relationship between the coding mechanism and low power consumption has attracted the attentions of researchers in various fields such as computer science, engineering, biology, and physics. Nature has evolved mechanisms for coding information and performing complex computations with minimal energy consumption. This has inspired the development of new approaches in engineering and computer science that aim to emulate nature's efficient coding mechanisms to achieve low power consumption. One example of such mechanisms is the use of spiking neural networks, which are based on the communication between neurons in the brain. Spiking neural networks are highly efficient in terms of energy consumption, and they have been used in various applications, including robotics and machine learning.

CRediT authorship contribution statement

Chenggui Yao: Investigation, Validation, Software, Data curation, Writing – review & editing, Visualization. **JianQiang Sun:** Software, Data curation, Writing – original draft. **Jun Jin:** Conceptualization, Methodology. **Jianwei Shuai:** Investigation, Writing – review & editing. **Xiang Li:** Investigation, Writing – review & editing, Visualization. **Yuangen Yao:** Conceptualization, Methodology, Validation, Writing – review & editing. **Xufan Xu:** Software.

Declaration of competing interest

The authors declare that they have no known competing financial interests or personal relationships that could have appeared to influence the work reported in this paper.

Data availability

Data will be made available on request.

Acknowledgments
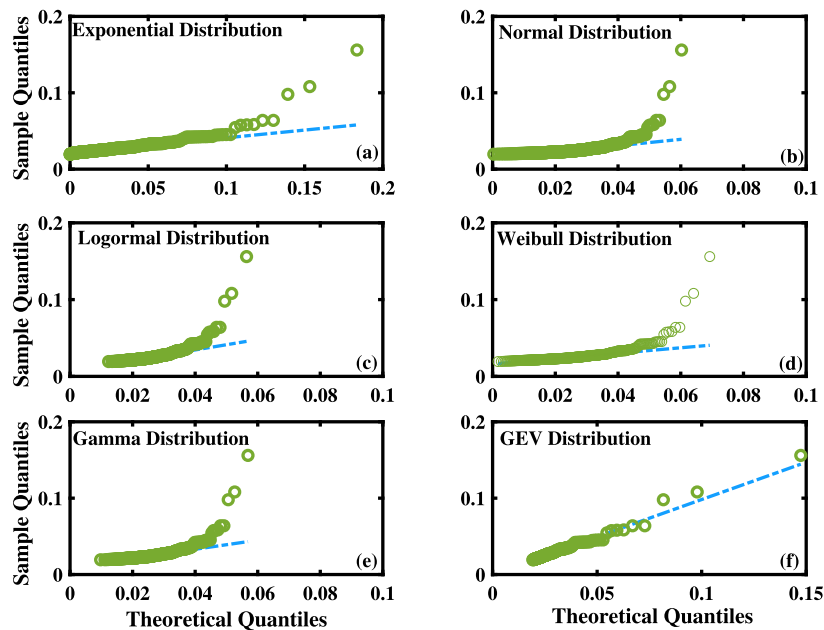
Fig. 10. (Color online) (a)–(f) Quantile–quantile plots that match the actual values with the following distributions respectively: Exponential, Normal, Lognormal, Weibull, Gamma and Generalized extreme value distribution (GEV). The data for the first spiking were obtained by sampling from a small-world network with chemical synapses under the following conditions: $N = 400$, $p_s = 0.3$, $\langle k \rangle = 4$, and $g_c = 0.5$.

References

[1] Rieke F, Warl D, Steveninck RR, Bialek W. Spikes exploring the neural code. Cambridge: MIT Press; 1999.

[2] Yao CG, He ZW, Nakano T, Shuai JW. Spiking patterns of a neuron model to stimulus: Rich dynamics and oxygen's role. Chaos 2018;28:083112.

[3] Yao CG, Xu F, Li XShuaiJW. Temperature-optimized propagation of synchronous firing rate in a feed-forward multilayer neuronal network. Physica A 2022;596:127139.

[4] Hopfield JJ. Pattern recognition computation using action potential timing for stimulus representation. Nature 1995;376:33–6.

[5] Vogels TP, Rajan K, Abbott L. Neural network dynamics. Annu Rev Neurosci 2005;28:357–76.

[6] Aertsen A, Diesmann M, Gewaltig MO. Propagation of synchronous spiking activity in feedforward neural networks. J physiol-Paris 1996;90:243–7.

[7] Mickey BJ, Middlebrooks JC. Representation of auditory space by cortical neurons in awake cats. J Neurosci 2003;23:8649–63.

[8] Wiener MC, Richmond BJ. Decoding spike trains instant by instant using order statistics and the mixture of Poissons model. J Neurosci 2003;23:2394–406.

[9] Wang H, Chen Y, Chen Y. First-spike latency in hodgkin's three classes of neurons. J Theoret Biol 2013;328:19–25.

[10] Shuai JW, Jung P. Entropically enhanced excitability in small systems. Phys Rev Lett 2005;95:114501.

[11] Ma J, Wang Y, Wang CN, Xu Y, Ren GD. Mode selection in electrical activities of myocardial cell exposed to electromagnetic radiation. Chaos Solition Fractals 2017;99:219–25.

[12] Shuai JW, Sheng R, Jung P. Entropically modified spiking ability and periodicity in clustered channels. Phys Rev E 2010;81:051913.

[13] Tan X, Wang X, Yang W, Xiao Z. First spike latency and spike count as functions of tone amplitude and frequency in the inferior colliculus of mice. Hear Res 2008;235:90–104.

[14] Wilson CD, Serrano GO, Koulakov AA, Rinberg D. A primacy code for odor identity. Nature Commun 2017;8(1477).

[15] Abraham NM, Spors H, Carleton A, Margrie TW, Kuner T, et al. Maintaining accuracy at the expense of speed: stimulus similarity defines odor discrimination time in mice. Neuron 2004;44:865–76.

[16] Muller D, Abel R, Brandt R, Zockler M, Menzel R. Differential parallel processing of olfactory information in the honeybee *Apis Mellifera L.*. J Compar Physiol A 2002;188:359–70.

[17] Krofczik S, Menzel R, Nawrot MP. Rapid odor processing in the honeybee antennal lobe network. Front Comput Neurosci 2009;2(9).

[18] Junek S, Kludt E, Wolf F, Schild D. Olfactory coding with patterns of response latencies. Neuron 2010;67:872–84.

[19] Joris PX, Smith PH, Yin TC. Neural processing of amplitude-modulated sounds. Physiol Rev 2006;86:1133–268.

[20] Berry MJ, Warl DK, Meister M. The structure and precision of retinal spike trains. Proc Natl Acad Sci 1997;94:5411–6.

[21] Furukawa S, Middlebrooks JC. Cortical representation of auditory space: information- bearing features of spike patterns. J Neurophysiol 2002;87:1749–62.

[22] Heil P. First-spike latency of auditory neurons revisited. Curr Opin Neurobiol 2004;14:461–7.

[23] Gawne T, Kjaer T, Richmond B. Latency: another potential code for feature binding in striate cortex. J Neurophysiol 1996;76:1356–60.

[24] Reich D, Mechler F, Victor J. Temporal coding of contrast in primary visual cortex: when what, and why. J Neurophysiol 2001;85:1039–50.

[25] Panzeri S, Petersen R, Schultz S, Lebedev M, Diamond M. The role of spike timing in the coding of stimulus location in rat somatosensory cortex. Neuron 2001;29:769–77.

[26] Petersen R, Panzeri S, Diamond M. The role of individual spikes and spike patterns in population coding of stimulus location in rat somatosensory cortex. Biosystems 2002;67:187–93.

[27] Spors H, Grinvald A. Spatio-temporal dynamics of odor representations in the mammalian olfactory bulb. Neuron 2002;34:301–15.

[28] Chase SM, Young ED. First-spike latency information in single neurons increases when referenced to population onset. Proc Natl Acad Sci 2007;104:5175–80.

[29] Paoli M, Albi A, Zanon M, Zanini D, Antolini R, et al. Neuronal response latencies encode first odor identity information across subjects. J Neurosci 2018;38:9240–51.

[30] Tuckwell HC. Spike trains in a stochastic hodgkin-huxley system. Biosystems 2005;80:25–36.

[31] Pankratova EV, Polovinkin AV, Spagnolo B. Suppression of noise in fitzhughnaguomo model driven by a strong periodic signal. Phys Lett A 2005;344:43–50.

[32] Pankratova E, Polovinkin A, Mosekilde E. Resonant activation in a stochastic hodgkin-huxley model: interplay between noise and suprathreshold driving effects. Eur Phys J B 2005;45:391–7.

[33] Ozer M, Grahaml L. Impact of network activity on noise delayed spiking for a hodgkin-huxley model. Eur Phys J B 2008;61:499–503.

[34] Uzuntarla M, Uzun R, Yilmaz E, Ozer M, Perc M. Noise-delayed decay in the response of a scale-free neuronal network. Chaos Solitons Fractals 2013;56:202–8.

[35] Ozer M, Uzuntarla M, Perc M, Graham LJ. Spike latency and jitter of neuronal membrane patches with stochastic Hodgkin–Huxley channels. J Theoret Biol 2009;261(1):83–92.

[36] Uzuntarla M, Ozer M, Guo D. Controlling the first-spike latency response of a single neuron via unreliable synaptic transmission. Eur Phys J B 2012;85(282).

[37] Ozer M, Uzuntarla M. Effects of the network structure and coupling strength on the noise- induced response delay of a neuronal network. Phys Lett A 2008;372:4603–9.

[38] Yao CG, He ZW, Luo JM, Shuai JW. Resonance induced by a spatially periodic force in the reaction–diffusion system. Phys Rev E 2015;91:052901.

[39] Yao CG, He ZW, Nakano T, Qian Y, Shuai JW. Inhibitory-autapse-enhanced signal transmission in neural networks. Nonlinear Dynam 2019;97:1425–37.

[40] Baysal V, Yılmaz E. Chaotic signal induced delay decay in Hodgkin–Huxley neuron. Appl Math Comput 2021;411:126540.

[41] Yu YG, Hill AP, McCormick DA. Warm body temperature facilitates energy efficient cortical action potentials. PLoS Comput Biol 2012;8:1002456.

[42] Song X, Wang H, Chen Y, Lai YC. Emergence of an optimal temperature in action-potential propagation through myelinated axons. Phys Rev E 2019;100:032416.

[43] Yao CG, Yao YG, Qian Y, Xu XF. Temperature-controlled propagation of spikes in neuronal networks. Chaos Solition Fractals 2022;164:112667.

[44] Sejnowski TJ, Paulsen O. Network oscillations: emerging computational principles. J Neurosci 2006;26:1673–6.

[45] Buzsaki G. Neural syntax: cell assemblies synapsembles, and readers. Neuron 2010;68(3):362–85.

[46] Telesford QK, Joyce KE, Hayasaka S, Burdette JH, Laurienti PJ. The ubiquity of small-world networks. Brain Connect 2011;5:367–75.

[47] Rubinov M, Knock SA, Stam CJ, Micheloyannis S, Harris AWF, et al. Small-world properties of nonlinear brain activity in schizophrenia. Hum Brain Mapping 2009;30:403–16.

[48] Bassett DS, Bullmore E. Small-world brain networks. Neuroscientist 2006;12:512–23.

[49] Tian LX, Wang JH, Yan CG, He Y. Hemisphere and gender-related differences in small world brain networks: A resting-state functional mristudy. NeuroImage 2011;54:191–202.

[50] Hilgetag CC, Goulas A. Is the brain really a small-world network. Brain Struct Funct 2015;221:2361–6.

[51] Stam C. Functional connectivity patterns of human magnetoencephalographic recordings: a 'small-world' network. Neurosci Lett 2004;355:25–8.

[52] Watts DJ, Strogatz SH. Collective dynamics of 'small-world' networks. Nature 1998;393:440–2.

[53] Sporns O, Zwi JD. The small world of the cerebral cortex. Neuroinformatics 2004;2:145–62.

[54] Ma J, Wang CN, Jin WY, Wu Y. Transition from spiral wave to target wave and other coherent structures in the networks of Hodgkin–Huxley neurons. Appl Math Comput 2010;217(8):3844–52.

[55] Clauset A, Shalizi CR, Newmani ME. Power-law distributions in empirical data. SIAM Rev 2004;51:661–703.

[56] Koshiya N, Smith JC. Neuronal pacemaker for breathing visualized in vitro. Nature 1999;400:360–3.

[57] Wang XJ. Pacemaker neurons for the theta rhythm and their synchronization in the septohippocampal reciprocal loop. J Neurophysiol 2002;87:889–900.

[58] Gu HG. Experimental observation of transition from chaotic bursting to chaotic spiking in a neural pacemaker. Chaos 2013;23:023126.

[59] Barabasi AL, Albert R. Emergence of scaling in random networks. Science 1999;286:509–12.

[60] Newman ME. Power laws pareto distributions and Zipf's law. Contemporary Phys. 2005;46:323–51.

[61] Hethcote HW. The mathematics of infectious diseases. SIAM Rev 2000;42:599–653.

[62] West GB, Brown JH, Enquist BJ. The fourth dimension of life: fractal geometry and allometric scaling of organisms. Science 1999;284:1677–9.